Surface & Coatings Technology 351 (2018) 212–219

Contents lists available at ScienceDirect

Surface & Coatings Technology

journal homepage: www.elsevier.com/locate/surfcoat

# Preparation of nickel–graphene composites by jet electrodeposition and the influence of graphene oxide concentration on the morphologies and properties

Lulu Ji[a], Feida Chen[a], Hai Huang[a], Xiangyu Sun[a], Yuanyuan Yan[a], Xiaobin Tang[a,b,*]

[a] Department of Nuclear Science & Engineering, Nanjing University of Aeronautics and Astronautics, Nanjing 210016, China
[b] Jiangsu Key Laboratory of Nuclear Energy Equipment Materials Engineering, Nanjing 210016, China

ARTICLE INFO

*Keywords:*
Nickel–graphene composite
Jet electrodeposition
Graphene oxide
Microhardness
Electrochemical corrosion properties

ABSTRACT

Nickel–graphene (N–G) composites are potential candidate structural materials for molten salt reactors. A rapid preparation method for these composites by jet electrodeposition was developed, and the microstructure, microhardness, and corrosion properties of these composites were studied to explore the key parameters of the jet electrodeposition. Results indicated that the distribution of graphene in composites mainly depended on the concentration of graphene oxide (GO) in the plating solution. Composites deposited with GO concentration of 0, 0.5, 1 g/L showed surface root-mean-square roughness value (Rq) of 6, 12, and 28 nm, respectively. Meanwhile with the increase of GO concentration, the Hardness value became larger. The corrosion potential $E_{corr}$ and current $I_{corr}$ of composites obtained at 0.5 g/L with the best surface quality were 193 mV and $5.7 \times 10^{-6}$ A/cm$^2$, respectively, which indicated the best electrochemical corrosion resistance. Hydrogen annealing can help self–repair of graphene microstructure.

## 1. Introduction

Nickel–graphene (Ni–G) composites are expected to supersede the Ni–based alloys owing to their remarkable radiation tolerance, and therefore, are potential structural candidate for advanced molten salt reactors [1–4]. However, the prominent challenge in the fabrication of high–performance Ni–G composites, especially the rapid preparation of a uniform dispersed graphene–reinforced Ni–based composite, restricts their practical application [5]. In recent years, researchers have prepared metal graphene composites by many different methods, such as powder metallurgy and electrodeposition [6–9]. Powder metallurgy is a relatively mature process to prepare metal composites, and suitable for producing near net block parts with complex geometry. However, the drawbacks of preparing graphene composites through this process are that the structure of graphene will be damaged during the high–energy ball milling process and gap defects are easily produced in the process of sintering [10, 11]. Meanwhile, electrodeposition can be operated at room temperature and atmospheric pressure. The grain size of the prepared materials is finer than that of powder metallurgy, and the materials show advanced mechanical and chemical properties due to the fine–grained strengthening of electrodeposition. However, the conventional electrodeposition technology has a poor deposition efficiency and therefore is not amenable for industrial production [12, 13].

In this study, a rapid deposition method for preparation of Ni–G composites by the jet electrodeposition is reported. Compared with the conventional electrodeposition technique, jet electrodeposition is a modified method with the advantages of high limit current and selective jet plating [14]. The circulating plating solution and jet can remarkably smoothen the surface and reduce the agglomeration of the second phase in the electrolyte [15, 16]. Moreover, the limit current can be substantially improved with the high-speed jet effectively reducing the diffusion layer thickness. Consequently, the resulting composites have few defects and refined grains (< 20 nm) [17]. Shen et al. [18, 19] conducted many studies on the preparation of nanocrystalline Ni and Ni–based nanocomposites (Ni–$SiO_2$, Ni–$CeO_2$) by jet electrodeposition, and the surface quality and performance of materials prepared by this technique is remarkably improved. However, reports on the jet electrodeposition of Ni–G composite are relatively rare due to the high preparation cost of graphene and the difficulties in transferring the graphene into metal matrix caused by the strong hydrophobicity [20].

In this work, graphene oxide (GO) was used as a substitute for graphene. GO is advantageous compared with other graphene

* Corresponding author at: Department of Nuclear Science & Engineering, Nanjing University of Aeronautics and Astronautics, Nanjing 210016, China.
*E-mail address:* tangxiaobin@nuaa.edu.cn (X. Tang).

https://doi.org/10.1016/j.surfcoat.2018.07.083
Received 18 May 2018; Received in revised form 22 July 2018; Accepted 29 July 2018
Available online 30 July 2018
0257-8972/ 

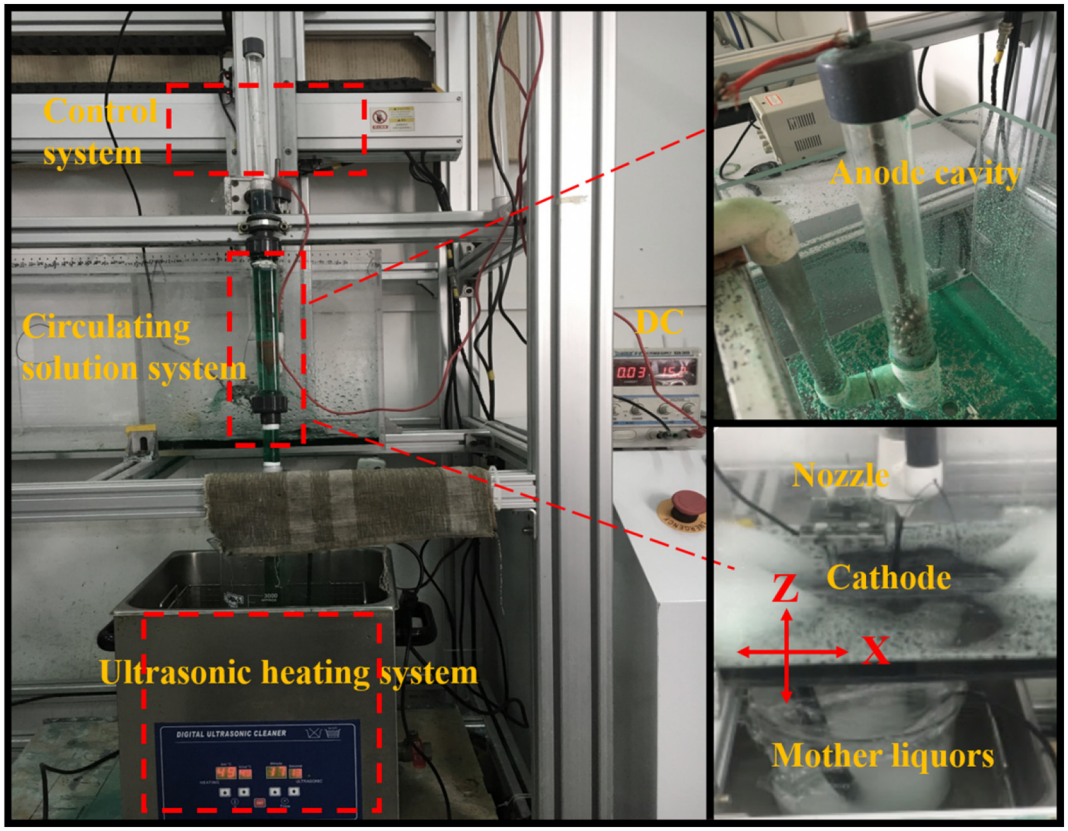


**Fig. 1.** Images of jet electrodeposition device.

derivatives due to its low cost, mass production, and hydrophilicity [21]. The Ni and Ni–G composites were prepared by jet electrodeposition and then the microstructure, microhardness, and electrochemical corrosion properties of these composites were studied.

## 2. Experiments and methods

### 2.1. Experiment system

This experiment adopted a jet electrodeposition method with the advantages of high limit current and selective jet plating. The images of the experimental system are shown in Fig. 1. The system consists of four main modules, namely control system, circulating solution system, ultrasonic heating system, and DC power. This system can realize the setting of electrodeposition range, scanning speed, and anode cathode distance and the control of the flow, bath temperature, and the layer thickness. The pump transfers the plating solution to the anode cavity and jets it to the cathode workpiece through a nozzle. Through the control system, the workpiece can move along the X–Z direction. Then, the plating solution flows back into the main liquid tank. All these processes ensure the stability and controllability of deposition.

### 2.2. Experimental details

#### 2.2.1. Preparation of the jet electrodeposition plating solutions

The Cu sheet was employed as the substrate material with dimensions of 50.0 mm × 30.0 mm × 0.20 mm. The GO in this study was an industrial monolayer GO (JCGO-95-1-2.6) purchased from Nanjing JCNANO Technology Co., Ltd. The jet electrodeposition plating solution was a modified Watts solution, and the main compositions are shown in Table 1. The reagents used in the experiment were all analytically pure. Fig. S1 shows the images of the jet electrodeposition plating solution after standing for 10 h.

**Table 1**
Composition of the jet electrodeposition plating solution.

| | Bath composition | Chemical reagents | Concentrations (g/L) |
|---|---|---|---|
| Basic solution | Metallic main salt | $NiSO_4{\cdot}6H_2O$ | 280 |
| | Anodic activator | $NiCl_2{\cdot}6H_2O$ | 35 |
| | pH buffer | $H_3BO_3$ | 40 |
| | The second phase | GO | 0, 0.5, 1 |
| Surfactant | Grain refiner | Saccharin | 0.8 |
| | Wetting agent | SDS | 0.1 |
| | Brightener | $C_4H_6O_2$ | 0.5 |

$NiSO_4{\cdot}6H_2O$ was the main salt providing the source of Ni in the plating solution. $NiCl_2{\cdot}6H_2O$ was employed as the anodic activator to improve the conductivity and dispersing ability of the plating solution. $H_3BO_4$ was utilized as the pH buffer. Sodium dodecyl sulfate (SDS) is essential for the Ni–G composite plating solution. The reaction between the SDS and GO can cause electrostatic saturation [22], which reduces the agglomeration of GO. Saccharin and $C_4H_6O_2$ were added to the plating solution as surfactant agents to obtain composites with good brightness, smoothness, and fine grain size.

#### 2.2.2. Fabrication of the Ni and Ni–G composites

Fig. 2 shows the jet electrodeposition process for the fabrication of the Ni and Ni–G composites. The copper (Cu) sheet and Ni were used as the cathode and anode, respectively. First, the Cu substrates were polished to obtain a mirror surface. The polished substrates were cleaned with acetone and alcohol. Then, the substrates were pretreated with degreasing solution and acidizing fluid in a 65 °C water bath for 5 min. Therefore, the plating solutions were prepared in accordance with Table 1 and then mixed for 2 h by mechanical stirring and ultrasonic heating at 50 °C. Finally, the jet electrodeposition device was prepared for the electrodeposition process. The process of jet electrodeposition is

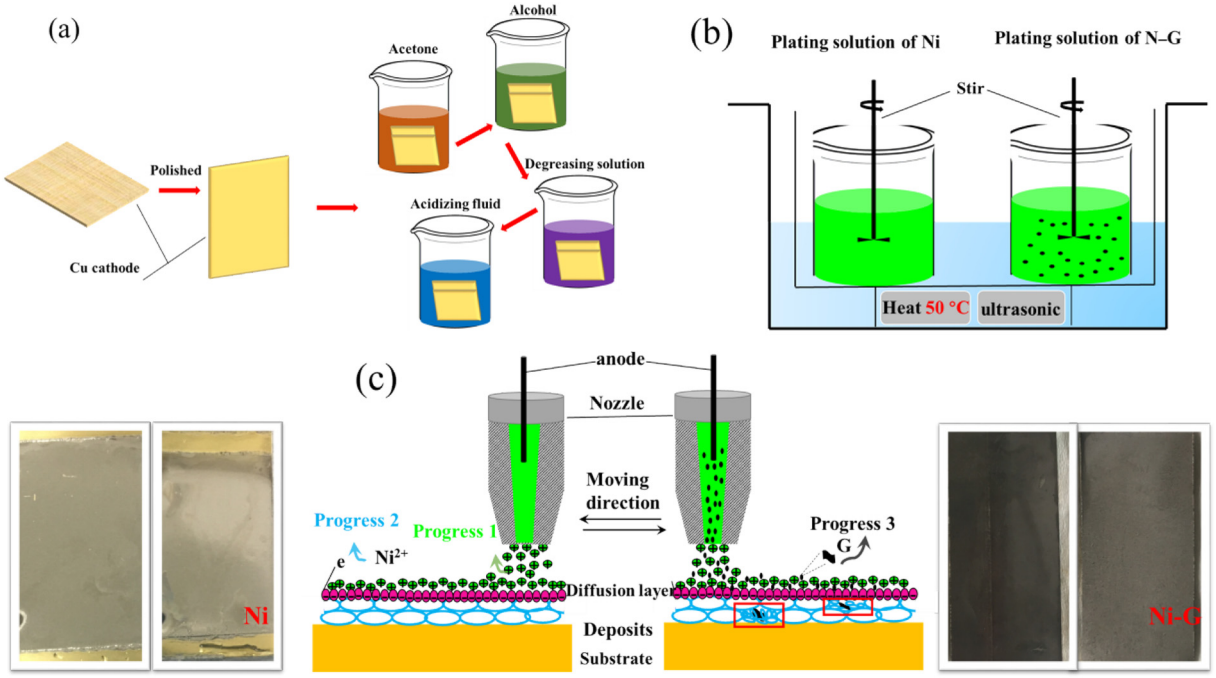


**Fig. 2.** Schematic of the jet electrodeposition process: (a) cathodic pretreatment process; (b) configuration process of Ni and Ni–G plating solution; (c) jet electrodeposition process and Ni and Ni–G composite samples.

embodied in supplementary video files. The deposition parameters are illustrated in Table 2.

The degreasing solution was a mixture of 10 g/L sodium sulfate ($Na_2SO_4$), 30 g/L sodium hydroxide (NaOH), 30 g/L sodium dihydrogen phosphate ($NaH_2PO_4$), and 30 g/L sodium phosphate ($Na_3PO_4$) and was used to remove the oil pollution on the substrate surface. The acidizing fluid of 20% hydrochloric acid (HCl) helped activate the surface for improved interfacial bonding. The reactions in the circulating solution system are shown in Fig. 2(c). In Process 1, the plating solution is continuously jetted onto the cathode surface through the nozzle, unlike in the traditional electrodeposition method. This practice is helpful to reduce the thickness of the diffusion layer ($\delta$) and increase the limiting current density ($D$). The equation can be expressed as follows:

$$D = nFk(C_s - C_0)/\delta \quad (1)$$

where $D$ is the limiting current density, n indicates the metal ion electron valence number, $F$ represents the Faraday constant ($9.6485 \times 10^4$), $C_s$ is the concentration of the solution near the cathode surface, $C_0$ stands for the solution concentration, and $\delta$ is the thickness of the diffusion layer. To the best of our knowledge, if the concentration difference is constant and current density is invariant, then the low $\delta$ value can increase $D$. In Process 2, the main salt releases $Ni^{2+}$ to take part in redox reaction on the substrate surface, where GO is co–deposited with Ni and embedded in Ni deposits, under the action of the electric current [23, 24]. In Process 3, GO forms structural defects due to the partial loss of oxygen functional groups (hydroxyl, carboxyl, and carbonyl). The graphene structure is also reorganized [25, 26].

Three kinds of materials were prepared, namely, Ni, Ni–G05, and Ni–G10, with different concentrations of GO in the plating solution. After cleaning with absolute ethyl alcohol and deionized water, the samples were dried and preserved. Parts of the materials were annealed with hydrogen (hydrogen volume of 5%, 500 °C, 10 °C/min, heat preservation time of 1 h), namely Ni(H), Ni–G05(H), and Ni–G10(H).

### 2.3. Characterization

The thickness and surface morphologies of the composites were characterized using a field emission scanning electron microscope (Apollo 300, Obducat CamScan Ltd., UK), which was equipped with energy dispersive spectrometer (EDS) to inspect the chemical compositions. The Ni–GO composites were etched for 5 min in ferric chloride solution to study the graphene microstructures inside the composites. The Raman spectra of the GO and the Ni–G composites before and after heat treatment were observed using a confocal Raman microscope (Renishaw, laser wavelength of 514 nm). Atomic force microscopy (AFM, Nanoscope IIIa) were used to obtain the surface structural morphologies and roughness quantitatively.

The mechanical properties were characterized by nano indentation (Nano Indenter G20, Agilent) with continuous stiffness method. Each sample was tested at three points with a depth of 2 μm.

The potentiodynamic polarization and the electrochemical impedance spectroscopy (EIS) were investigated in 3.5 wt% sodium chloride (NaCl) using an electrochemical workstation model CHI660E (CH Instrument, Inc., Shanghai, China). The traditional three-electrode system was used. In particular, the saturated calomel electrode was as the reference electrode, the platinum as the auxiliary electrode, and the sample of 1 $cm^2$ as the working electrode. The open circuit potential (OCP) was measured for 30 min before the subsequent experiments. The polarization experiments were measured in the range from −0.2 V to 1 V (versus the stable OCP) with a scanning rate of 1 mV/s. The impedance was performed with a frequency from 0.01 Hz to 100KHz. Furthermore, the sinusoidal amplitude was 10 mV.

**Table 2**
Parameters of the jet electrodeposition process.

| pH | T | Current density | Electrodeposition time | Flow | Anode–cathode distance (Z) | Electrodeposition range (X) |
|---|---|---|---|---|---|---|
| 3.5–4.5 | 50 °C | 100 A/$dm^2$ | 5, 20, and 150 min | 400 L/h | 2 mm | 10 and 30 mm |

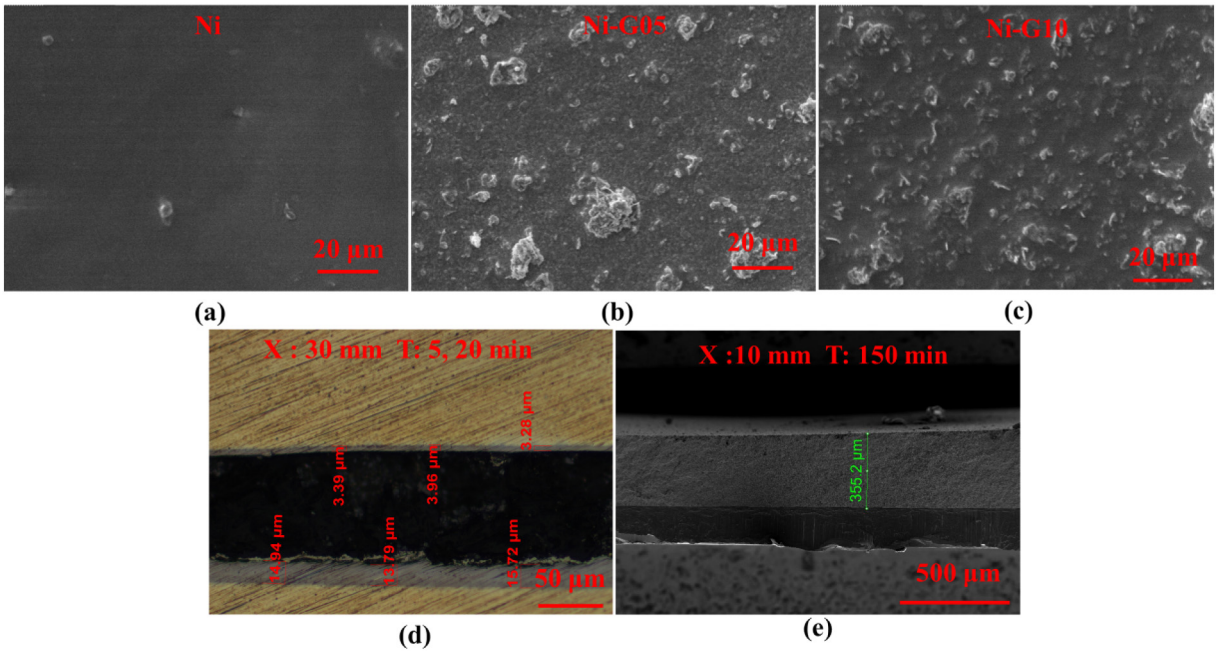


**Fig. 3.** Surface morphologies of the materials as electrodeposited: (a–c) top-view SEM images of the Ni, Ni–G05, and Ni–G10; (d–e) cross-sectional thickness of different electrodeposition parameters.

## 3. Results and discussion

### 3.1. Surface morphologies of the Ni and Ni–G composites

Fig. 3(a–c) show the top-view SEM images of Ni, Ni–G05, and Ni–G10 prepared by jet electrodeposition for comparison. As shown in Fig. 3(a), Ni probably is the smoothest and most compact. The addition of 0.5 g/L GO caused the slight surface fluctuation, with some impurities as demonstrated in Fig. 3(b). As the GO concentration increased to 1 g/L, some large surface fluctuation with a uniform distribution of GO agglomerations was observed. Besides, the more precise analysis was also carried out using AFM analysis. The three types of composites (Ni, Ni–G05, and Ni–G10) were evaluated by surface root-mean-square roughness values (Rq) which were 6, 12, and 28 nm, respectively in a scanned area of 5 μm × 5 μm in Fig.4. Clearly, the surface roughness of the materials increased with the increase in the GO concentration.

The change in morphology possibly due to the introduction of GO. According to the growth process of the Ni and Ni–G as shown in Fig. 2(c), Ni ions ($Ni^{2+}$) trapped the electrons and undergone redox reactions along the smooth substrate surface. When the substrate surface was completely covered by the deposits, the redox reaction continued above it. GO was co-deposited with Ni and embedded in the deposits. Some barrier interfaces were formed near the graphene sheets, which affected the normal growth of Ni grains. Therefore, the inhomogeneous growth of Ni grains near the graphene increased the surface roughness.

Unlike the traditional electrodeposition process, controlling the movement of the cathode along the X direction can change the deposition range. The thickness of the deposit can be controlled by changing the electrodeposition time (T). As shown in Fig. 3(d), two samples were mosaicked in the opposite position, so the thickness of the coating can be observed clearly from the cross-section image. The yellow part in the image is the copper basement, the black part is the mosaic material and the gray part is the coating material. From the image, we can see the thickness of the deposits with electrodeposition time (T) of 5 and 20 min is about 3 and 12 μm, respectively. The SEM of

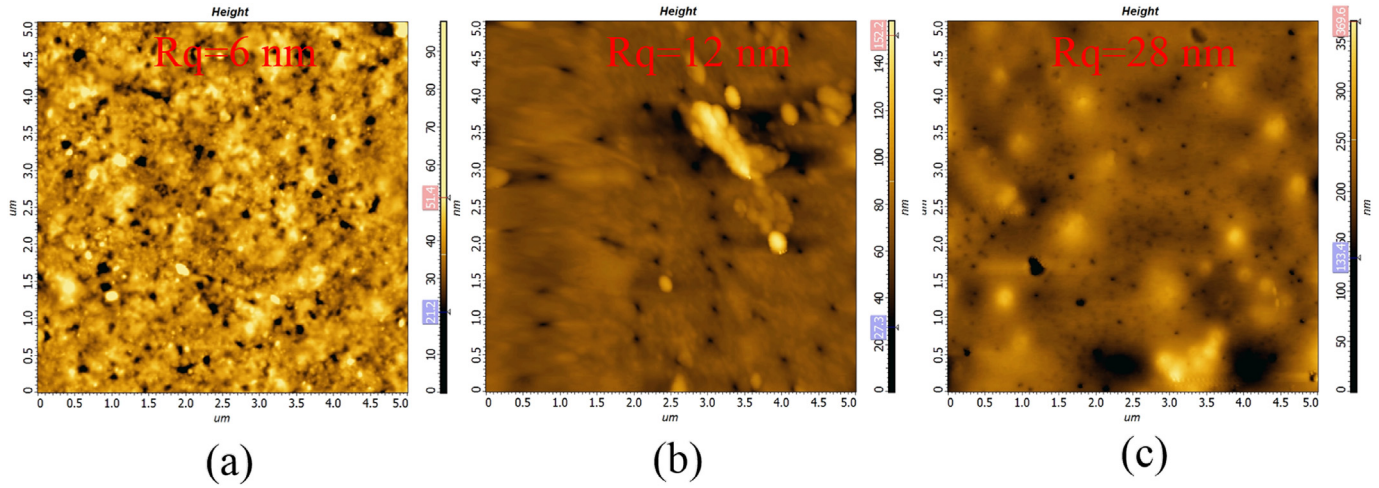


**Fig. 4.** AFM images and surface root-mean-square roughness value (Rq) of the materials as electrodeposited: (a) Ni, (b) Ni–G05, (c) Ni–G10.

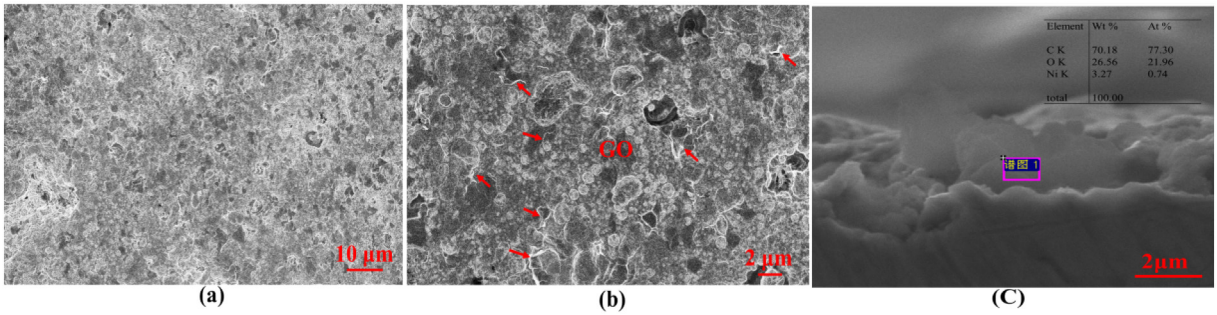


**Fig. 5.** Microstructures of the Ni–G05: (a–b) top-view SEM images of Ni–G05 after corrosion at low and high magnifications; (c) EDS detected from the surface of Ni–G05.

Fig. 3(e) shows that the plating thickness can reach about 350 μm, when the electrodeposition time is extended to 150 min and the electrodeposition range(X) is changed. At the same time, it can be clearly seen that the thickness of the coating material is relatively uniform and the cross-section structure is compact.

### 3.2. Microstructures of the Ni–G composites

Fig. 5(a–b) show the internal microstructure of Ni–G composites after corrosion. A large number of semitransparent graphene sheets were uniformly embedded in the Ni matrix. These sheets helped in the second phase dispersion strengthening of the composites. Fig. 5(c) determines the local chemical composition of Ni–G05, where Ni, C, and O accounted to approximately 70 wt%, 27 wt% and 3 wt%, respectively. To a certain extent, GO had successfully incorporated into the Ni–G composites.

The XRD patterns of Ni, Ni–G05 and Ni–G10 are presented in Fig. 6. The diffraction peaks at 2θ = 44°, 52°, are assigned to (111) and (200) crystalline structures of Ni. The average crystallite sizes of the coatings were estimated using Scherrer equation as below:

$$\beta = \frac{K\lambda}{L\cos\theta}\cdot\frac{180^{\circ}}{\pi} \quad (2)$$

where $\beta$ is the full width half maxima (FWHM) of the (111) diffraction in 2θ degree, $K$ is Scherrer constant (0.87 used here), λ is the wavelength of Cu-Kα radiation (0.154 nm), $\theta$ is the diffraction angle, $L$ is the crystallite size in nm. the calculated values were compared in Table 3. The result shows that after adding GO, the average grain size of the material is about 1/3 of pure nickel. Compared with Ni–G05, the (111) peak and (200) peak of Ni–G10 attenuated, indicating that with the increase of GO concentration, the defects in the electrodeposition process increased, and the crystallinity of the materials became worse.

**Table 3**
Calculated crystallite size by Scherrer's equation of Ni, Ni–G05 and Ni–G10.

| Sample | θ | hkl plane | FWHM | Average L (nm) |
|---|---|---|---|---|
| Ni | 44.45 | (111) | 0.156 | 49.2 |
| | 51.76 | (200) | 0.205 | |
| Ni-G05 | 44.31 | (111) | 0.515 | 15.1 |
| | 51.67 | (200) | 0.662 | |
| Ni-G10 | 44.35 | (111) | 0.601 | 13.2 |
| | 51.63 | (200) | 0.750 | |

Fig. 7 shows the Raman spectra of the original GO and Ni–G composites before and after hydrogen annealing. As shown in the figure, the D and G peaks appeared at around 1355 and 1585 $cm^{-1}$, which indicated the disorders in the carbon skeleton and the graphene intrinsic sp2–conjugated structure [27]. The calculated ratios of Ni–G05 and Ni–G10 before hydrogen annealing were 0.96 and 0.90, respectively, which were increased compared with the original GO (0.78). The reason might be due to the distortion of GO sheets during electrodeposition process and the loss of oxygen-containing functional groups that could increase the defects, thereby resulting in the disorder of the GO structure. The calculated ratios after hydrogen of Ni–G05(H) and Ni–G10(H) were 0.74 and 0.76, respectively. This decrease in the $I_D/I_G$ ratio after hydrogen annealing (Ni–G05: 0.74 vs. 0.90, Ni–G10: 0.76 vs.

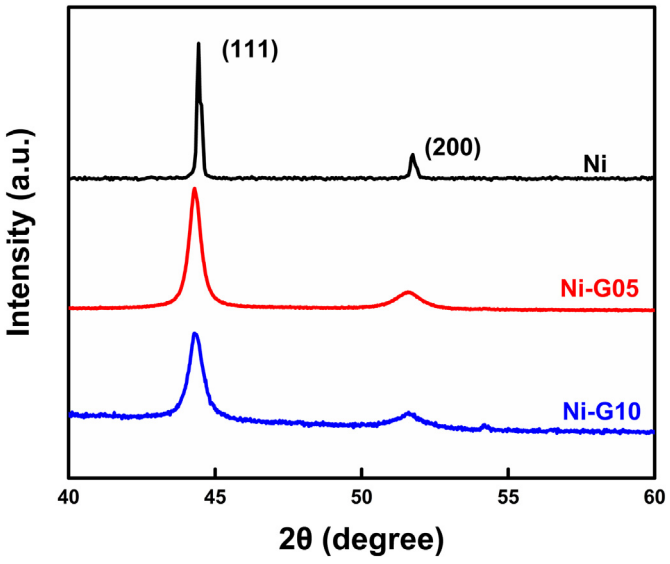


**Fig. 6.** XRD patterns of Ni, Ni–G05 and Ni–G10.

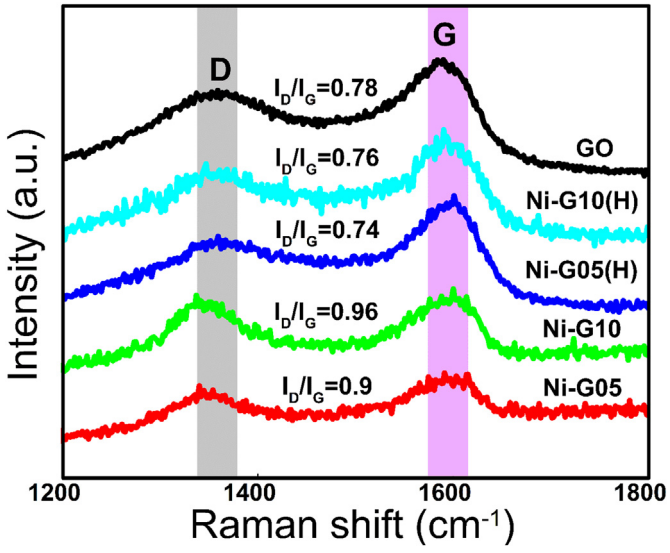


**Fig. 7.** Comparison of the Raman spectra of the GO and Ni–G composites before and after hydrogen annealing.

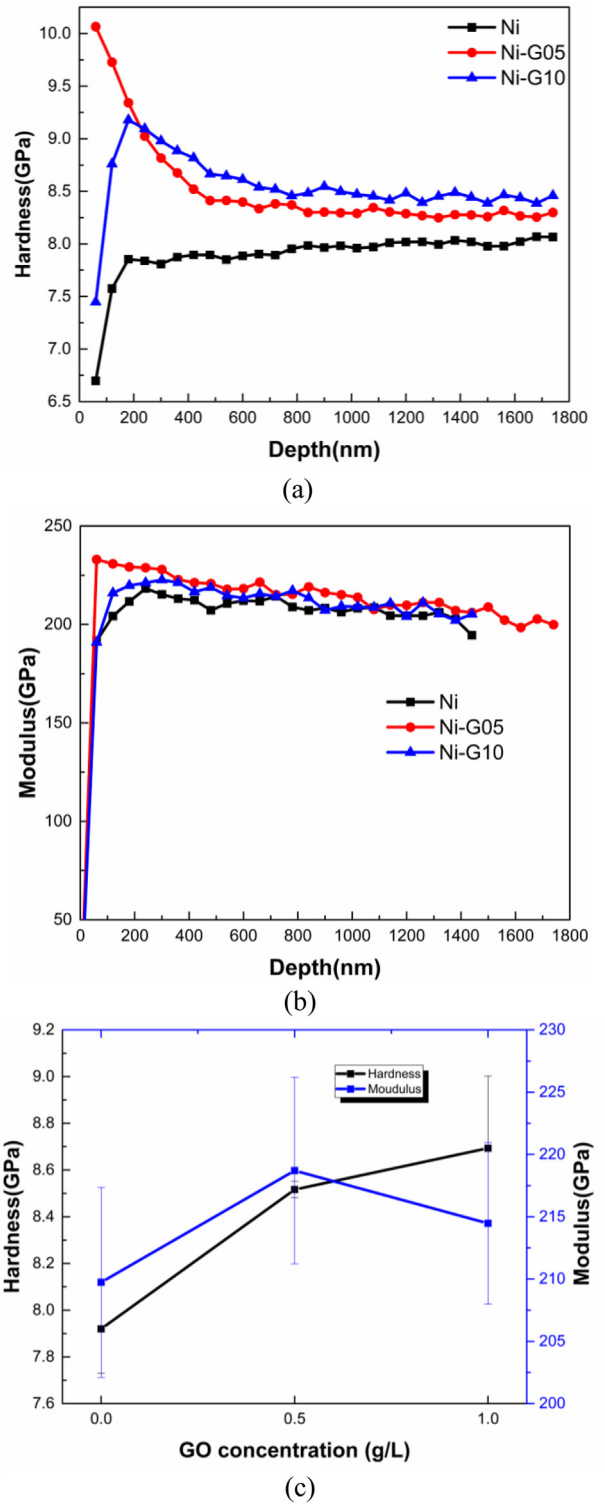


**Fig. 8.** Hardness-depth curves (a) and modulus-depth curves (b) of Ni, Ni–G05, Ni–G10 and corresponding average value and standard deviation of hardness and modulus (c) of the materials.

0.96) indicated that the self-repairing of the graphene structure had occurred during hydrogen annealing, and the average size of the sp2 domain had been increased [26, 28].

### 3.3. Mechanical properties of the Ni and Ni–G composites

Hardness is a comprehensive expression of resistance to deformation, friction and wear. Therefore, its value is an important parameter to study the mechanical properties of metal composites. Nanoindentation is a well-developed method for determining hardness and Young's modulus values of composites which can minimize the influence due to the substrate.

Fig. 8(a–c) shows the average hardness–depth and modulus–depth curves of Ni, Ni–G05 and Ni–G10. The details of the relevant nanoindentation test are shown in Figs. S2–S4 of the Supporting material. It can been seen that the mechanical properties of the materials were positively related to the GO concentration, especially the nanoindentation hardness showed obvious hardening effect. The Vickers hardness test in Fig. S5 also shows this trendency. Although this method

**Table 4**
Statistics of test mechanical performance results (average value).

| Sample | Nano-hardness (GPa) | Modulus (GPa) | Vickers hardness (HV0.025) |
|---|---|---|---|
| Ni | 7.92 | 210 | 531 |
| Ni–G05 | 8.52 | 219 | 603 |
| Ni-G10 | 8.70 | 214 | 629 |

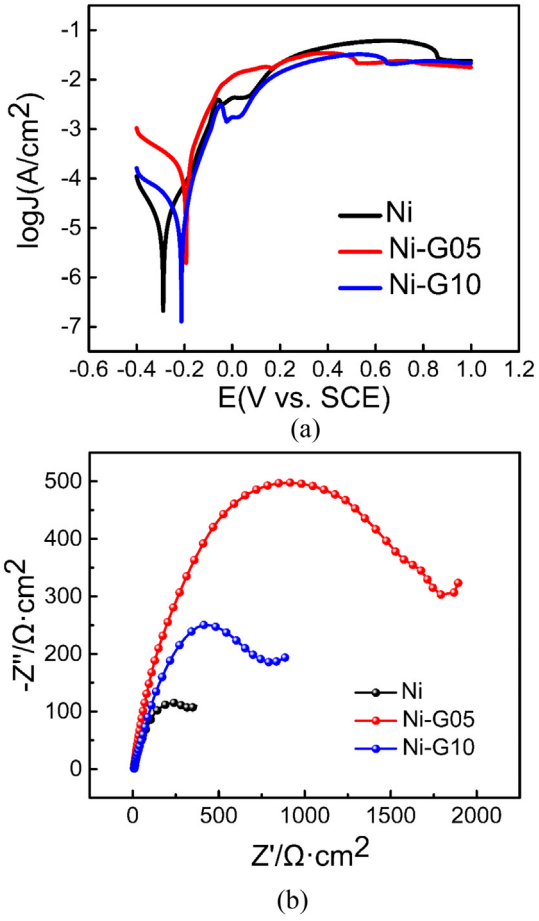


**Fig. 9.** Electrochemical corrosion properties in 3.5 wt% NaCl solution: (a) polarization curves and (b) Nyquist plots of EIS for Ni, Ni–G05, and Ni–G10 composites.

**Table 5**
Calculated Tafel characteristics from the polarization curves.

| Sample | $E_{corr}$ (mV vs. SCE) | $j_{corr}$ ($\times 10^{-6}$ A/cm$^2$) |
|---|---|---|
| Ni | −289 | 14.4 |
| Ni–G05 | −193 | 5.7 |
| Ni–G10 | −213 | 20.3 |

is easy to be affected by brass substrate, the hardness is less than the actual value.

In the process of nanoindentation test, when the indenter is pressed into the material at the shallow position, the measurement result has serious size effect and the test is unstable. Therefore, the relative mechanical properties of the deeper segment are calculated in Table 4. The result shown average nanoindentation hardness/moudulus of 7.92/210 GPa, 8.52/219 GPa and 8.70/214 GPa for Ni, Ni–G05 and Ni–G10, respectively. Additionally, the nanoindentation hardness and modulus prepared by conventional electrodeposition are 1.81 GPa and 166.70 GPa, respectively [6]. Compared with the traditional electrodeposition process, the jet electrodeposition process has the characteristics of high speed jet and high current density. Therefore, pure nickel (Ni) prepared by jet electrodeposition process is more compact and has better mechanical properties.

The remarkable increase of nanoindentation hardness should be related to the grain refinement of nickel matrix shown in Table 3, which is a common way for the strengthening of a material. In an electrochemical deposition process the nucleation and crystal growth compete against each other. The GO embedded in the nickel matrix (Fig. 5), thus hindering the normal growth of nickel grains, and providing nucleation sites for new grains.The incorporated GO sheets could demonstrate an anchor effect which prevent nickel grain sliding and plastic deformation, thus enhancing the mechanical properties [29–31]. Moreover the intrinsic mechanical strength of GO sheets might have a contribution to the enhancement.However, it has been reported that the mechanical properties of GO sheets are affected by the degree of structural defects [32, 33]. When the concentration of GO is beyond a specific level (for instance Ni–G10 in this work), the agglomeration will occur, the electrical reduction is not complete and so on, resulting in the instability of mechanical properties, even worse than the pure nickel.

### 3.4. Electrochemical corrosion properties of the Ni and Ni–G composites

As shown in the polarization curves in Fig. 9(a), the corrosion potentials $E_{corr}$ of Ni–G05 and Ni–G10 considerably shifted to the right compared with that of Ni, thereby indicating a better corrosion resistance tendency. The partial fluctuation of the corrosion current in the positive potential region might be due to the local defects in the materials. Table 5 shows the calculated Tafel data. The results showed that the corrosion current density $j_{corr}$ of Ni–G05 decreased compared with that of Ni ($5.7 \times 10^{-6}$ A/cm$^2$ vs. $14.4 \times 10^{-6}$ A/cm$^2$), whereas the $j_{corr}$ of Ni–G10 increased to $20.3 \times 10^{-6}$ A/cm$^2$. This finding reflected that the corrosion rate of Ni–G10 was faster than that of Ni. Considering the surface morphologies mentioned above, the graphene in Ni–G10 formed a large amount of agglomeration in Ni matrix, thereby resulting in a rough surface. In this way, the corrosive solution could easily penetrate through the surface.

The EIS can accurately reflect the electrochemical corrosion properties. Fig. 9(b) shows the Nyquist plots of EIS for Ni, Ni–G05, and Ni–G10 composites. Ni–G05 showed the largest semi-circular arc. In general, the larger the impedance arc, the better the reflection of the corrosion resistance [34]. Two small semicircular arcs in Ni–G10 were observed probably because the deposit was penetrated quickly and the Cu substrate was corroded.

## 4. Conclusions

The Ni and Ni–G composites were successfully prepared by jet electrodeposition. The effects of electrodeposition parameters and GO concentration on the surface morphology and properties of graphene composites were investigated. The related characterization results showed that the jet electrodeposition technology could increase the limiting current density ($D$) and prepare composites with different sizes to meet the practical application as far as possible. Proper hydrogen annealing helped the self-repair of the graphene structure.

The distribution of graphene in composites mainly depended on the concentration of GO in the plating solution. Excessive GO caused agglomeration, and the surface roughness of the material increased. Ni–G05 had a better surface quality than Ni–G10.

The hardness and electrochemical experiments showed that a proper amount of GO could effectively improve the mechanical and corrosion resistance of the graphene composites. The improvement of the properties was due to the dispersion strengthening of GO and the grain refinement near the graphene, but the excessive GO adversely affected the properties. In this study, Ni–G05 had the best comprehensive performance. To further enhance the performance of Ni–G composites, the parameters of the jet electrodeposition process should be further optimized.

Supplementary data to this article can be found online at https://doi.org/10.1016/j.surfcoat.2018.07.083.

## Acknowledgements

This work was supported by the National Natural Science Foundation of China (Grant No. 11705087), the Natural Science Foundation of Jiangsu Province (Grant No. BK20170776), and the Foundation of Graduate Innovation Center in NUAA (Grant No. kfjj20170609).

## References

[1] S. Si, W. Li, X. Zhao, M. Han, Y. Yue, W. Wu, S. Guo, X. Zhang, Z. Dai, X. Wang, Significant radiation tolerance and moderate reduction in thermal transport of a tungsten nanofilm by inserting monolayer graphene, Adv. Mater. 29 (2016).
[2] H. Huang, X. Tang, F. Chen, J. Liu, H. Li, D. Chen, Graphene damage effects on radiation-resistance and configuration of copper-graphene nanocomposite under irradiation: A molecular dynamics study, Sci. Rep. 6 (2016), https://doi.org/10.1038/srep39391.
[3] H. Huang, X. Tang, F. Chen, Y. Yang, J. Liu, H. Li, D. Chen, Radiation damage resistance and interface stability of copper-graphene nanolayered composite, J. Nucl. Mater. 460 (2015) 16–22, https://doi.org/10.1016/j.jnucmat.2015.02.003.
[4] J. Zeng, J. Liu, H.J. Yao, P.F. Zhai, S.X. Zhang, H. Guo, P.P. Hu, J.L. Duan, D. Mo, M.D. Hou, Y.M. Sun, Comparative study of irradiation effects in graphite and graphene induced by swift heavy ions and highly charged ions, Carbon 100 (2016) 16–26, https://doi.org/10.1016/j.carbon.2015.12.101.
[5] K. Fu, X. Zhang, C. Shi, E. Liu, F. He, J. Li, N. Zhao, C. He, An approach for fabricating Ni@graphene reinforced nickel matrix composites with enhanced mechanical properties, Mater. Sci. Eng. A 715 (2018) 108–116, https://doi.org/10.1016/j.msea.2017.12.101.
[6] D. Kuang, L. Xu, L. Liu, W. Hu, Y. Wu, Graphene-nickel composites, Appl. Surf. Sci. 273 (2013) 484–490, https://doi.org/10.1016/j.apsusc.2013.02.066.
[7] Z. Xu, X. Shi, W. Zhai, J. Yao, S. Song, Q. Zhang, Preparation and tribological properties of TiAl matrix composites reinforced by multilayer grapheme, Carbon 67 (2014) 168–177, https://doi.org/10.1016/j.carbon.2013.09.077.
[8] C.L.P. Pavithra, B.V. Sarada, K.V. Rajulapati, T.N. Rao, G. Sundararajan, A new electrochemical approach for the synthesis of copper-graphene nanocomposite foils with high hardness, Sci. Rep. 4 (2014), https://doi.org/10.1038/srep04049.
[9] J. Wang, Z. Li, G. Fan, H. Pan, Z. Chen, D. Zhang, Reinforcement with graphene nanosheets in aluminum matrix composites, Scr. Mater. 66 (2012) 594–597, https://doi.org/10.1016/j.scriptamat.2012.01.012.
[10] Y. Chen, X. Zhang, E. Liu, C. He, C. Shi, J. Li, P. Nash, N. Zhao, Fabrication of in-situ grown graphene reinforced Cu matrix composites, Sci. Rep. 6 (2016) 19363.
[11] H. Yue, L. Yao, X. Gao, S. Zhang, E. Guo, H. Zhang, X. Lin, B. Wang, Effect of ball-milling and graphene contents on the mechanical properties and fracture mechanisms of graphene nanosheets reinforced copper matrix composites, J. Alloys Compd. 691 (2017) 755–762.
[12] T. Borkar, S.P. Harimkar, Effect of electrodeposition conditions and reinforcement content on microstructure and tribological properties of nickel composite coatings, Surf. Coat. Technol. 205 (2011) 4124–4134.
[13] S. Qi, X. Li, Z. Zhang, H. Dong, Fabrication and characterisation of electro-brush plated nickel-graphene oxide nano-composite coatings, Thin Solid Films 644 (2017).
[14] F. Xia, W. Jia, M. Jiang, W. Cui, J. Wang, Microstructure and corrosion properties of Ni-TiN nanocoatings prepared by jet pulse electrodeposition, Ceram. Int. 43 (2017).
[15] H. Goel, P.M. Pandey, Performance evaluation of different variants of jet electrochemical micro-drilling process, Proc. Inst. Mech. Eng. B J. Eng. Manuf. 232 (2016).
[16] M.S. Rajput, P.M. Pandey, S. Jha, Modelling of high speed selective jet electrodeposition process, J. Manuf. Process. 17 (2015) 98–107.
[17] C. Wang, L. Shen, M. Qiu, Z. Tian, W. Jiang, Characterizations of Ni-CeO 2 nanocomposite coating by interlaced jet electrodeposition, J. Alloys & Compd. 727 (2017).
[18] W. Zhuo, L. Shen, M. Qiu, Z. Tian, W. Jiang, Effects of flexible friction on the properties of nanocrystalline nickel prepared by jet electrodeposition, Surf. Coat.

Technol. 333 (2017) 87–95.
[19] X. Liu, L. Shen, M. Qiu, Z. Tian, Y. Wang, K. Zhao, Jet electrodeposition of nanocrystalline nickel assisted by controllable friction, Surf. Coat. Technol. 305 (2016) 231–240.
[20] S.J. An, Y. Zhu, H.L. Sun, M.D. Stoller, T. Emilsson, S. Park, A. Velamakanni, J. An, R.S. Ruoff, Thin film fabrication and simultaneous anodic reduction of deposited graphene oxide platelets by electrophoretic deposition, J. Phys. Chem. Lett. 1 (2015) 258–266.
[21] A. Siokou, F. Ravani, S. Karakalos, O. Frank, M. Kalbac, C. Galiotis, Surface refinement and electronic properties of graphene layers grown on copper substrate: an XPS, UPS and EELS study, Appl. Surf. Sci. 257 (2011) 9785–9790.
[22] C. Guo, Y. Zuo, X. Zhao, J. Zhao, J. Xiong, Effects of surfactants on electrodeposition of nickel-carbon nanotubes composite coatings, Surf. Coat. Technol. 202 (2008) 3385–3390.
[23] L. Chen, Y. Tang, K. Wang, C. Liu, S. Luo, Direct electrodeposition of reduced graphene oxide on glassy carbon electrode and its electrochemical application, Electrochem. Commun. 13 (2011) 133–137.
[24] Y. Shao, J. Wang, M. Engelhard, C. Wang, Y. Lin, Facile and controllable electrochemical reduction of graphene oxide and its applications, J. Mater. Chem. 20 (2010) 743–748.
[25] Y. Jin, B. Hu, Z. Wei, Z. Luo, D. Wei, Y. Xi, Y. Zhang, Y. Liu, Roles of H2 in annealing and growth times of graphene CVD synthesis over copper foil, J. Mater. Chem. A 2 (2014) 16208–16216.
[26] N.J. Song, C.X. Lu, C.M. Chen, C.L. Ma, Q.Q. Kong, Effect of annealing temperature on the mechanical properties of flexible graphene films, New Carbon Mater. 32 (2017) 221–226.
[27] S. Stankovich, D.A. Dikin, R.D. Piner, K.A. Kohlhaas, A. Kleinhammes, Y. Jia, Y. Wu, S.B.T. Nguyen, R.S. Ruoff, Synthesis of graphene-based nanosheets via chemical reduction of exfoliated graphite oxide, Carbon 45 (2007) 1558–1565.
[28] H. Zhang, X. Zhang, D. Zhang, X. Sun, H. Lin, C. Wang, Y. Ma, One-step electrophoretic deposition of reduced graphene oxide and Ni(OH)2 composite films for controlled syntheses supercapacitor electrodes, J. Phys. Chem. B 117 (2013) 1616–1627.
[29] M.H. Allahyarzadeh, M. Aliofkhazraei, A.R. Rezvanian, V. Torabinejad, A.R.S. Rouhaghdam, Ni-W electrodeposited coatings: characterization, properties and applications, Surf. Coat. Technol. 307 (2016) 978–1010.
[30] M. Allahyarzadeh, M. Aliofkhazraei, A.S. Rouhaghdam, V. Torabinejad, Electrodeposition of multilayer Ni-W and Ni-W-alumina nanocomposite coatings, Surf. Eng. 33 (2017) 327–336.
[31] M.H. Allahyarzadeh, M. Aliofkhazraei, A.R.S. Rouhaghdam, V. Torabinejad, Structure and wettability of pulsed electrodeposited Ni-W-Cu-(α-alumina) nanocomposite, Surf. Coat. Technol. 307 (2016) 525–533.
[32] T. Borkar, S. Harimkar, Microstructure and wear behaviour of pulse electrodeposited Ni–CNT composite coatings, Surf. Eng. 27 (2013) 524–530.
[33] Q. Zheng, Z. Li, Y. Geng, S. Wang, J.K. Kim, Molecular dynamics study of the effect of chemical functionalization on the elastic properties of graphene sheets, J. Nanosci. Nanotechnol. 10 (2010) 7070–7074.
[34] K. Jiang, J. Li, J. Liu, Electrochemical codeposition of graphene platelets and nickel for improved corrosion resistant properties, RSC Adv. 4 (2014) 36245–36252.